



University of Wisconsin - Madison

Madison, WI 53706

November 1994

# Observations on the Potential Confinement of a Light Fermion

M. G. Olsson and Sinisa Veseli

Department of Physics, University of Wisconsin, Madison, WI 53706

Ken Williams

Continuous Electron Beam Accelerator Facility

Newport News, VA 23606, USA

and

Physics Department, Hampton University, Hampton, VA 23668

## Abstract

We consider possible dynamical models for a light fermion confined by a potential well. With the Dirac equation only Lorentz scalar confinement yields normalizable wavefunctions, while with the "no pair" variant of the Dirac equation only Lorentz vector confinement has normal Regge behaviour. A systematic investigation of Regge properties and phenomenological properties is carried out, including calculations of the Isgur-Williams function. We point out that the Isgur-Williams function provides a sensitive test of confinement models. In particular, the slope of the IW function at zero recoil point is found to be  $\alpha(1)' = 0.90$  for the Dirac equation with scalar confinement, and  $\alpha(1)' = 1.20$  for the no pair equation with vector confinement. Using heavy-light data alone we argue against scalar confinement.

# 1 Introduction

The description of the dynamical confinement of a light fermion by a central force requires an examination of various wave equations. For example, the direct application of the Dirac equation with Lorentz vector confinement leads to pair production on hadronic time scales which is not observed. In this case the "no pair" (NP) or "quenched" variant of the Dirac equation is used to obtain a physical and "well posed" result.

In this paper we survey the solutions of the Dirac and NP equation for both Lorentz vector and scalar confining potentials. We use the results in each case to compare to heavy-light meson data. Dirac scalar confinement and NP vector confinement are capable of accounting for the measured meson masses as well as the Isgur-Wise function. The values of the parameters resulting from the fits however provide interesting clues to the correct form of the confinement. In particular, we will argue against scalar confinement on the basis of heavy-light data alone.

We begin in Section 2 with a brief discussion of one particle fermionic wave equations and their properties. Classical arguments reveal the Regge behaviour and categorize the effects of the negative energy states on the positive energy solutions. In Section 3 we discuss our numerical method and reproduce the pure Coulomb NP solution of Hardekopf and Sucher [1]. We then successively consider scalar and vector confined mesons with Dirac and NP equations in Section 4 and we summarize our findings in Section 5.

## 2 Wave equations

The time independent Dirac equation for a quark of mass  $m$  moving in a Lorentz scalar potential  $S(r)$  and the time component of a Lorentz vector potential  $V(r)$  is

$$[\mathbb{H}_0 + P \cdot \mathbb{E}] \psi(r) = 0 ; \quad (1)$$

where the free particle Dirac Hamiltonian is

$$H_0 = \alpha \mathbf{p} + \beta m ; \quad (2)$$

and

$$P(\mathbf{r}) = V(\mathbf{r}) + S(\mathbf{r}) ; \quad (3)$$

$E$  is the energy of the "light degrees of freedom", and  $\alpha$  and  $\beta$  are the usual Dirac matrices [2].

When one attempts to use the Dirac equation to solve the Helium atom one finds [1, 3] that no normalizable solutions are possible. This "continuum dissociation" is a form of the Klein paradox when the negative energy states mix with the positive energy states. Since Helium clearly exists, one must rephrase the Dirac equation to suppress this mixing. The result is the NP equation [1].

An analogous phenomenon occurs for a single particle moving in an increasing (confining) Lorentz vector potential. For a very long time [4] it has been realized that there are no normalizable solutions to the Dirac equation in this case. This again is an example of the Klein paradox [5]. For a potential which rises sufficiently fast and a sufficiently small quark mass, the states corresponding to the free negative and positive energies mix resulting in the loss of normalizability. In both these cases a simple alteration to the Dirac equation avoids this mixing. The free Dirac Casimir projection operators [2] are

$$P_{\pm} = \frac{E_0 \pm H_0}{2E_0} ; \quad (4)$$

where

$$E_0 = \sqrt{\mathbf{p}^2 + m^2} ; \quad (5)$$

These projection operators have the well known properties,

$$P_{\pm}^2 = P_{\pm} ; \\ P_+ + P_- = 1 ;$$

$$+ + = 1 ; \tag{6}$$

$$H_0 = H_0 :$$

If  $+$  acts on the Dirac equation (1) from the left we obtain by use of (6)

$$+ (H_0 + P E) = [H_0 + + P ( + + ) E + ] = 0 : \tag{7}$$

The term represents pair production in the interaction [1]. The NP approximation is obtained by dropping the term. Defining a new wave function

$$= + ; \tag{8}$$

the resulting NP equation is

$$(H_0 + P_+ E) = 0 ; \tag{9}$$

where

$$P_+ = + P + : \tag{10}$$

## 2.1 Classical turning points

The s-wave classical turning points provide valuable insight into the structure of these wave equations. By inspection, some vital properties of the solutions will be evident. The s-wave turning points are defined by  $p = 0$  in (1) and (9). The turning point condition for the Dirac equation (1) is

$$(m + S) + V = E : \tag{11}$$

There are two turning points; one bounding the positive energy states ( $= 1$ ) and the other bounding the negative energy states when  $= 1$ . They are

$$E_+ = m + S(r) + V(r) ; \tag{12}$$

$$E_- = m - S(r) + V(r) : \tag{13}$$

We consider in turn scalar confinement [ $V = 0; S = ar$ ] and vector confinement [ $V = ar; S = 0$ ]. The s-wave turning points given in (12) and (13) are plotted in Figs. 1 and 2 for scalar and vector confinement respectively. The two cases are dramatically different. The scalar confinement turning points insure separation of the positive and negative state regions resulting in a well defined mathematical problem. The vector confinement turning points plotted in Fig. 2 allow the free negative energy states to rise into the positive energy region causing mixing for a given positive energy. This mixing is known as the Klein paradox [5]. In principle this means there are no normalizable bound states although for heavy quarks the mixing effect is negligible.

At the s-wave turning point we have

$$+ (p = 0) = \begin{pmatrix} 0 & 1 \\ 1 & 0 \\ 0 & 0 \end{pmatrix} A ; \quad (14)$$

and the NP turning points from (9) are given by

$$E_+ = m + S(r) + V(r) ; \quad (15)$$

$$E_- = -m ; \quad (16)$$

These are plotted in Fig. 3 and are the same for scalar and vector confinement. From this point of view vector confinement has become a well defined concept since normalizable bound states are now expected to exist.

## 2.2 Spherical solutions

Because of spherical symmetry, we look for the solution in the form [2]

$$\begin{pmatrix} 0 & 1 \\ 1 & 0 \end{pmatrix} \begin{pmatrix} f_j^k(r) Y_{jm}^k(\hat{r}) \\ ig_j^k(r) Y_{jm}^k(\hat{r}) \end{pmatrix} A ; \quad (17)$$

where

$$\mathbb{Y} = \begin{pmatrix} 0 & 1 \\ Y_{jm}^k & 0 \\ 0 & iY_{jm}^k \end{pmatrix} A ; \quad (18)$$

and  $Y_{jm}^k$  are the spherical spinors. Using the identity

$$pY_{jm}^k = iY_{jm}^k D ; \quad (19)$$

where

$$D = \frac{k}{r} + \left( \frac{d}{dr} + \frac{1}{r} \right) ; \quad (20)$$

and

$$D = D_+^Y ; \quad (21)$$

which can be verified by integration by parts. We commute the  $Y$  matrix to the left to obtain the standard coupled radial equations,

$$(\mathbb{h}_0 + P - E) \begin{pmatrix} f_j^k \\ g_j^k \end{pmatrix} A = 0 ; \quad (22)$$

where

$$\mathbb{h}_0 = \begin{pmatrix} 0 & 1 \\ m & D \\ D_+ & m \end{pmatrix} A ; \quad (23)$$

$$P = \begin{pmatrix} 0 & 1 \\ V + S & 0 \\ 0 & V - S \end{pmatrix} A ; \quad (24)$$

The quantum number  $k$  labels the meson and is defined by

$$k = \left( j + \frac{1}{2} \right) ; \quad (25)$$

where the + sign means  $l = j + \frac{1}{2}$  or  $k = l$ , the - sign means  $l = j - \frac{1}{2}$  or  $k = (l + 1)$ , and hence  $l(l + 1) = k(k + 1)$ .

An analogous pair of coupled first order radial equations, can be obtained for the NP equation (9). We define

$$= \frac{E_0^k - m}{2E_0^k} ; \quad (26)$$

where  $E_0^k$  is to be evaluated using orbital angular momentum  $l$  according to (25), i.e.

$$E_0^k = \sqrt{p_r^2 + \frac{k(k+1)}{r^2} + m^2} ; \quad (27)$$

The identity

$$+ \mathbb{Y} = \mathbb{Y} L ; \quad (28)$$

with

$$L = \frac{B}{e} \left( D + \frac{1}{2E_0^k} \right) + \frac{1}{2E_0^k} D \frac{C}{A} ; \quad (29)$$

then gives the radial NP equation

$$(\mathbb{m}_0 + L P L - E_1)^e \begin{pmatrix} f_j^k \\ g_j^k \end{pmatrix} = 0 ; \quad (30)$$

It should be noted from (21) and (29) that  $L^y = L$ .

The radial equations for the Dirac case (22) or the NP case (30) are solved in a similar manner as discussed in Section 3. The NP equation can of course be thought of as a Dirac equation with a coordinate and momentum dependent potential.

### 2.3 Regge behaviour

In the ultra-relativistic limit one aspect of the Dirac solutions can be inferred immediately without any detailed calculation. For large orbital angular momenta the Regge trajectories become linear for linear confinement and have a slope that is characteristic of the Lorentz nature of the confinement. The result that the single light quark Regge slopes are exactly double the corresponding two light quark

Regge slopes should be noted [6], where in each case the energy in the Regge slope is identified as the excitation energy (i.e., meson energy minus heavy quark mass).

We consider high rotation  $|j| \gg 1$  and nearly circular orbits. The radial Dirac equation (22) then implies

$$\frac{g_j^k}{f_j^k} = \frac{V + S}{\frac{k}{r}} \frac{E}{V - S - E} = \frac{\frac{k}{r}}{V - S - E}; \quad (31)$$

which becomes

$$(E - V)^2 - S^2 = \frac{k^2}{r^2}; \quad (32)$$

The state of the lowest energy for a fixed  $k$  satisfies  $\frac{\partial E}{\partial r} = 0$ , or

$$(E - V)^2 V^0 + S S^0 = \frac{k^2}{r^3}; \quad (33)$$

The two cases we are considering are

Scalar component:  $S = ar; V = 0$ , for which

$$\alpha_0 = \frac{|j|}{E^2} = \frac{1}{2a}; \quad (34)$$

Vector component:  $S = 0; V = ar$ , giving a Regge slope of

$$\alpha_0 = \frac{|j|}{E^2} = \frac{1}{4a}; \quad (35)$$

The Regge behaviour of the NP equation proceeds similarly. By (20), (26) and (27) the high  $|j| \gg 1$  limit implies that

$$L(|j| \gg 1) = \frac{1}{2} \begin{pmatrix} 0 & 1 \\ \hat{k} & 1 \end{pmatrix} \hat{k}_A; \quad (36)$$

where  $\hat{k} = \frac{k}{|j|}$ , and the NP equation potential term is

$$\begin{aligned} L P L &= \frac{1}{4} \begin{pmatrix} 0 & 1 \\ \hat{k} & 1 \end{pmatrix} \hat{k}_A \begin{pmatrix} 1 & 0 \\ 0 & V + S \end{pmatrix} \begin{pmatrix} 1 & 0 \\ A & \hat{k} \end{pmatrix} \\ &= \frac{1}{2} V(r) \begin{pmatrix} 0 & 1 \\ \hat{k} & 1 \end{pmatrix} \hat{k}_A; \end{aligned} \quad (37)$$



We first note that the scalar potential cancels in this limit and hence the universal Regge behaviour is lost with NP scalar confinement. The radial equation (30) then yields

$$\frac{g_j^k}{f_j^k} = \frac{E + \frac{1}{2}V}{\hat{k} \left( \frac{j^k}{r} + \frac{1}{2}V \right)} = \frac{\hat{k} \left( \frac{j^k}{r} + \frac{1}{2}V \right)}{E + \frac{1}{2}V} : \quad (38)$$

The solutions are  $E = -\frac{j^k}{r}$  and a positive solution

$$E = V(r) + \frac{j^k}{r} : \quad (39)$$

For the positive solution the minimum  $E$  for a fixed  $k$  condition then gives

$$0 = \frac{j^k}{E^2} = \frac{1}{4a} : \quad (40)$$

This is identical to the Dirac vector confinement slope (35).

We note that although the origin of the NP equation lies in nearly non-relativistic atomic physics it retains vector confinement in the ultra-relativistic limit. The status of scalar confinement is drastically different. The situation here is reminiscent of the scalar confinement catastrophe which occurs in the momentum space formulation [7] where confinement is lost.

### 3 Description of the numerical method

Instead of solving (22) by integrating differential equations, we choose a variational (Galerkin) method [8]. We expand  $f_j^k$  and  $g_j^k$  in terms of a complete set of basis states  $\chi_n(r)$ , and truncate the expansion to the lowest  $N$  basis functions, i. e.

$$f_j^k(r) = \sum_{n=1}^N C_n^{(f)} \chi_n(r) ; \quad (41)$$

and

$$g_j^k(r) = \sum_{n=1}^N C_n^{(g)} \chi_n(r) : \quad (42)$$

Substituting these expressions into (22) or (30), and then multiplying from the left by

$$\int_0^z r^2 dr \quad (43)$$

we end up with a  $2N \times 2N$  matrix equation in the form

$$\begin{pmatrix} 0 & 1 & 0 \\ E & C^f & A \\ & C^g & \end{pmatrix} = \begin{pmatrix} H_{11} & H_{12} \\ H_{21} & H_{22} \end{pmatrix} \begin{pmatrix} C^f \\ C^g \end{pmatrix} = H \begin{pmatrix} C^f \\ C^g \end{pmatrix} : \quad (44)$$

Here,  $H_{ij}$  are symmetric  $N \times N$  matrices, and  $H_{12} = H_{21}^T$ . Diagonalizing the Hamiltonian matrix yields energies and eigenvectors in terms of the basis states. The lowest  $N$  energies and eigenvectors correspond to negative energy states, while the  $N + 1$  to  $2N$  states describe positive energy states. Basis states, and therefore energies and eigenvectors of  $H$ , depend on the variational size parameter  $\alpha$ . The dependence on  $\alpha$  of the lowest positive energy states (as well as the highest negative energy states) should vanish with increasing number  $N$  of basis states used. The pseudo-Coulombic basis states and all matrix elements used are described in Appendix A.

The Galerkin finite basis method will approach the true eigenvalues from above if the Hamiltonian matrix is positive definite. Although the Hamiltonians which we are considering here are not positive definite they still exhibit plateaus in  $E$ , which become wider as the number of basis states increases. In those cases where analytical or alternative numerical solutions are available our Galerkin plateaus correspond to the correct eigenvalues.

In order to see how the variational method works with the Dirac equation, we first solve pure Coulomb potential,

$$S(r) = 0 ; \quad (45)$$

$$V(r) = -\frac{1}{r} ; \quad (46)$$

for which the analytical solution is known [2]. In Fig. 4 we show dependence of the three lowest positive energy states (for  $m = 1$  GeV,  $\alpha = 0.5$ ,  $k = 1$  and  $j = \frac{1}{2}$ ) on

the variational parameter  $\alpha$ . The full lines represent the exact analytic solution of the Dirac equation. As we increase the number of basis states, the plateau region of  $\alpha$  where the eigenvalues of  $H$  are the same as the exact energies enlarges. The variational scheme works well in this case.

In Fig. 5 we illustrate the scaled energy of the ground state,

$$\epsilon = \frac{E - m}{2m}; \quad (47)$$

as a function of the Coulomb constant  $Z$ . The solid line shows the exact analytic Dirac result,

$$E = m \frac{1 - Z^2}{2}; \quad (48)$$

and also our numerical solution which are the same to high accuracy, even for values of  $Z$  close to one. The dashed line is the Coulomb NP equation ground state energy. As Hardekopf and Sucher [1] found the NP and Dirac solution are nearly the same for small  $Z$ . Our NP Coulomb solution is consistent with that obtained by Hardekopf and Sucher [1].

## 4 Results

### 4.1 Dirac equation with scalar confinement

Properties of the spectrum of the Dirac equation with scalar confinement and a short range Coulomb interaction have already been investigated in [9]. These authors also report results of their numerical calculations, which we have used as another check of our method. With  $N = 25$  basis states we were able to reproduce all of their numerical results for the eigenvalues to their given accuracy of four decimal places.

As in [9], we take

$$\begin{aligned} S(r) &= \alpha r; \\ V(r) &= -\frac{Z}{r}; \end{aligned} \quad (49)$$

but here we go a little bit further in investigating the use of the Dirac equation with scalar confinement in the description of heavy-light mesons. First, we make sure that nothing in our final result depends on the value of variational parameter  $\beta$ . In Fig. 6 we show the three lowest positive energy states and the three highest negative energy states for  $m_q = 0.3 \text{ GeV}$ ;  $a = 0.2 \text{ GeV}^2$ ;  $\beta = 0.5$ ;  $k = 1$  and  $j = \frac{1}{2}$ . Clearly, with  $N = 15$  we have a large region where the eigenvalues do not depend on  $\beta$ .

Next, we perform a systematic fit to the observed spin averaged heavy-light meson states. We fix the light quark mass to be  $m_{u,d} = 0.3 \text{ GeV}$ , and vary all the other parameters of the model to best account for the experimental data. In Table 1 we show the results of this fit, with parameters

$$\begin{aligned}
m_{u,d} &= 0.300 \text{ GeV (fixed)} ; \\
m_s &= 0.463 \text{ GeV} ; \\
m_c &= 1.301 \text{ GeV} ; \\
m_b &= 4.639 \text{ GeV} ; \\
a &= 0.308 \text{ GeV}^2 ; \\
\beta &= 0.579 :
\end{aligned} \tag{50}$$

As seen from the Table 1, the agreement with experimental data is excellent, and values of parameters are all reasonable, except for the value of the tension  $a$ .

From the universal Regge slope  $\alpha_0 = 0.8 \text{ GeV}^{-2}$ , one expects  $a$  to be

$$a = \frac{1}{2\alpha_0} = 0.2 \text{ GeV}^2 ; \tag{51}$$

and this is consistent with the value found from analyses of heavy quonia spectroscopies [8]. However, as we saw in (34), the Regge slope for the Dirac equation with scalar confinement is  $\alpha_0 = \frac{1}{2a}$ , so that tension necessary to account for the spin averaged meson masses must be about a factor of  $\frac{1}{2}$  larger than the one expected from light-light spectroscopies and the Nambu slope (51). Indeed, if we divide value of  $a$  from (50) by  $\frac{1}{2}$ , we get 0.2, as we expected.

As we have already mentioned, Regge slope for the Dirac equation with scalar confinement is expected to be  $\alpha' = \frac{1}{2a}$ . In order to verify this numerically, we fix  $a$  to be  $0.2 \text{ GeV}^{-2}$ , choose  $m_q = 0$ , and then plot dependence of  $j$  with respect to  $\frac{E^2}{2a}$ . As seen on the Fig. 7, slope of the Regge trajectories is one, as expected.

Once the wave functions are known for a heavy light meson the Isgur-Wise function, describing the semi-leptonic  $B \rightarrow D^{(*)}$  decay distribution, can be evaluated [10, 11]. Using

$$\langle D^{(*)} | \bar{\psi} \psi | B \rangle = \frac{2}{\Gamma + 1} \int_0^1 dr r^{\Gamma} R_D(r) R_B(r); \quad (52)$$

where

$$\langle B | \bar{\psi} \psi | B \rangle = \int_0^1 dr r^{\Gamma} R^2(r) A(r) R(r); \quad (53)$$

we find IW function that this model predicts. As shown on the Fig. 8, the agreement with ARGUS [12] and CLEO [13] data is reasonable. To calculate the slope, we use expression [11]

$$\alpha'(1) = \frac{1}{2} + \frac{1}{3} E_q^2 \langle r^2 \rangle; \quad (54)$$

For the range of light quark masses from 0 to  $350 \text{ MeV}$ , we obtain

$$\alpha'(1) = 0.90 \pm 0.02; \quad (55)$$

## 4.2 Dirac equation with vector confinement

If a fermion is confined by a Lorentz vector interaction, i. e.

$$\begin{aligned} S(r) &= 0; \\ V(r) &= \frac{1}{r} + ar; \end{aligned} \quad (56)$$

the Dirac equation has no normalizable solutions. As we mentioned earlier this has been known to be the case for over sixty years [4]. The origin of the problem is in the mixing between positive and negative energy states as shown in Fig. 2. Since the basis wavefunctions are all normalizable in our variational method it is of interest

to see how this problem is manifest. In Fig. 9 we show the  $\rho$ -plot with vector confinement for the three lowest positive and the three highest negative energy states. We see how the three states mix in the region of  $\rho$  where there should be a plateau. It is interesting to note however that if one extends the apparent plateaus through the level repulsions a consistent result is obtained which is not too different from the NP result below. The largest difference is in the ground state where Dirac and NP are about 50 MeV apart.

### 4.3 NP equation with scalar confinement

We observed in (37) that for large orbital excitation the NP scalar interaction cancels from the NP equation. The consequent loss of linear Regge trajectories eliminates any conventional discussion of meson states in terms of scalar confinement in the NP framework.

### 4.4 NP equation with vector confinement

There is reason to hope that the NP equation with vector confinement (56) will eliminate this mixing and hence reestablish a one particle wave equation. Comparing the s-wave turning point structure of the NP equation in Fig. 3 with the Dirac equation shown in Fig. 2 we observe that the NP negative energy states should not seriously mix with the positive energy states.

We proceed to the numerical solution of the NP equation (30) by the Galerkin method. In Fig. 10 we show the dependence on  $\rho$  of the three lowest positive and three highest negative energy solutions with  $m_q = 0.3 \text{ GeV}$ ;  $a = 0.2 \text{ GeV}^2$ ;  $\beta = 0.5$ ;  $k = 1$  and  $j = \frac{1}{2}$ . Again we observe a robust plateau structure which widens as the number of basis functions increases.

The Regge slope of the NP equation with vector confinement was shown in (40) to be  $\alpha^0 = \frac{1}{4a}$ . Our numerical solution agrees as shown in Fig. 11. In this figure

we illustrate the leading trajectories for the two light degrees of freedom states corresponding to  $k = (j + \frac{1}{2})$  for  $m_{u,d} = 0.3 \text{ GeV}$ ;  $a = 0.2 \text{ GeV}^2$  and  $\alpha = 0.5$ . We also show several daughter trajectories corresponding to radial excitations.

In order to recover the universal Regge slope, the tension in this case must be about  $\frac{1}{4}$  times the one from equation (51). Therefore, we fix  $a$  to be  $0.16 \text{ GeV}^2$ , choose  $m_{u,d} = 0.3 \text{ GeV}$  and fit to the spin averaged heavy-light meson states. Result is shown in Table 2, and parameters of the fit are

$$\begin{aligned}
 m_{u,d} &= 0.300 \text{ GeV} \quad (\text{fixed}) ; \\
 m_s &= 0.600 \text{ GeV} ; \\
 m_c &= 1.342 \text{ GeV} ; \\
 m_b &= 4.679 \text{ GeV} ; \\
 a &= 0.157 \text{ GeV}^2 \quad (\text{fixed}) ; \\
 \alpha &= 0.676 ;
 \end{aligned} \tag{57}$$

The agreement of the fitted levels to experiment is very good and comparable to the Dirac scalar confinement fit of Table 1.

Finally we use the wavefunctions with parameters of (57) to evaluate the IW function using (52). The result is shown on Fig. 12. The slope of the Isgur-Wise function at the zero recoil point is evaluated using (54) to be

$$\langle \Gamma \rangle(1) = -1.20 \pm 0.03 ; \tag{58}$$

where the error is estimated from the variation of the light quark mass  $0.25 < m_{u,d} < 0.35 \text{ GeV}$ . We observe that this slope is significantly more negative than the one found from the Dirac equation with scalar confinement (55), even though the same set of spin averaged heavy-light meson masses were used in the fit. However, if we compare Figs. 8 and 12, we see that Isgur-Wise function obtained from the NP equation agrees with the data a bit better than the one calculated from the Dirac equation with scalar confinement.

## 5 Conclusions

We have considered here the motion of a fermion in a central field. The interaction that we have emphasized is scalar or vector linear confinement. We are particularly interested in this problem because of its application to the description of heavy-light mesons. The wave equations considered are the Dirac equation and the "no pair" equation. Although the properties of the Dirac equation are well known we reconsider them in the light of a confining interaction and also to serve as benchmark for the related NP equation. Our main results are:

### 1. Dirac equation with scalar linear confinement

This is the most straightforward confinement model for a fermion. We find that it is a well posed problem with a unique solution and that by adjusting quark masses, Coulomb constant  $\alpha$ , and tension  $a$ , an excellent fit to heavy-light masses can be found. The tension found ( $a \approx 0.31 \text{ GeV}$ ) is larger than normally obtained from heavyonia fits and this may be viewed as evidence against scalar confinement. The origin of this discrepancy is the scalar confinement Regge slope  $\alpha' = \frac{1}{2a}$ . The slope is fixed by the p-wave heavy-light states and yields a tension about 50% larger than the usual value. If we force the tension to be  $0.2 \text{ GeV}^2$  then although the fit to the energy levels is still good, the Isgur-Wise function becomes shallow with a slope  $\alpha'(1) \approx 0.70$  and does not fit the experimental data well. We conclude that although scalar confinement gives mathematically consistent solutions, it does not seem to agree well with experiment.

### 2. Dirac equation with vector confinement

There are no normalizable bound state solutions in this case.

### 3. NP equation with scalar confinement



Scalar confinement in the no pair equation does not yield normal quasi-linear Regge trajectories and hence does not correspond to universal Regge behaviour.

#### 4. NP equation with vector confinement

This model of fermionic confinement also is viable. Vector NP confinement, along with an attractive Coulombic short range interaction, again gives good fits to the data. Vector confinement yields a Regge slope of  $\alpha^0 = \frac{1}{4a}$ , one half of the scalar value.

There are thus two alternative confinement models yielding linear Regge trajectories: scalar Dirac and vector NP. They both account for the data well. The differences though are interesting. The parameters, most notably the tension, are different when fitted to the data.

As we observed in Section 2.3 the Regge slope for scalar and vector confinement differ by a factor of two. Since the tension appears both in s-wave dynamics and in rotational states experimental data will ultimately decide the correct result. The tension preferred by heavyonia actually lies between the scalar Dirac and vector NP heavy-light values. As we have pointed out [14, 15] the heavy-light Regge slope  $\alpha^0 = \frac{1}{a}$  obtained in the relativistic flux tube model is consistent with the heavyonia value.

Another piece of information which should soon shed additional light on the proper model of confinement is the Isgur-Wise function. Both by experiment and from the lattice simulation of QCD, accurate values of the IW function (or its slope at zero recoil point) will be available. The Isgur-Wise function appears to depend fairly sensitively on the confinement model. As we have seen, Dirac scalar confinement yields  $\alpha^0(1) = 0.9$ , while NP vector confinement gives  $\alpha^0(1) = 1.2$ . Both of these models provide excellent fits to the same data set.

Finally, we should mention that we have been led into these questions by our investigation of the relativistic flux tube model [14, 15, 16]. For low orbital angular momentum states the flux tube model is similar to vector confinement. It appears from the results presented here that a NP type equation will be appropriate for the flux tube with one light fermion.

## A Basis states

The pseudo-Coulombic radial basis states are those used in previous calculations [8, 14, 15],

$$R_{i1}(r) = N_{i1}^{-\frac{3}{2}} (2-r)^1 e^{-r} L_i^{2l+2}(2-r); \quad (59)$$

where

$$N_{i1} = \frac{v}{u} \frac{8(i!)}{(i+2l+2)!}; \quad (60)$$

In these equations we assume  $0 \leq i \leq N-1$ . For computational precision and efficiency, the matrix representation of all operators have been calculated analytically

[17]. For  $p_r^2 = \frac{1}{r} \frac{\partial^2}{\partial r^2} r$ ,  $r$ ,  $\frac{1}{r}$  and  $\frac{1}{r^2}$  we have

$$p_r^2 i_{ij} = \left[ \frac{1}{2} i_{ij} + 2 \frac{N_{j1}}{N_{i1}} \frac{1(2l+3)(j-i) + (l+1)(2i+2l+3)}{(2l+1)(2l+3)} \right] i_{ij}; \quad (61)$$

$$h r i_{ij} = \frac{1}{2} (2i+2l+3) i_{ij} - \frac{1}{2} \frac{j(j+2l+2)}{i(i+2l+2)} i_{ij-1} + \frac{1}{2} \frac{j(j+2l+2)}{i(i+2l+2)} i_{ij+1}; \quad (62)$$

$$\frac{1}{r} i_{ij} = \frac{N_{j1}}{(l+1)N_{i1}} i_{ij}; \quad (63)$$

$$\frac{1}{r^2} i_{ij} = \frac{2^{-2}}{(l+1)(2l+1)(2l+3)} \frac{N_{j1}}{N_{i1}} [(2l+1)(j-i) + 2j+2l+3] i_{ij}; \quad (64)$$



## References

- [1] G. Hardekopf and J. Sucher, *Phys. Rev. A* 30, 703 (1984); *Phys. Rev. A* 31, 2020 (1985).
- [2] F. Gross, *Relativistic Quantum Mechanics and Field Theory*, John Wiley & Sons, Inc., 1993.
- [3] G. E. Brown and G. Ravenhall, *Proc. R. Soc. London A* 208, 552 (1951).
- [4] Milton S. Plesset, *Phys. Rev.* 41, 278 (1932).
- [5] J. D. Bjorken and S. D. Drell, *Relativistic Quantum Mechanics*, McGraw-Hill, Inc., 1964.
- [6] C. Goebel, D. LaCourse, and M. G. Olsson, *Phys. Rev. D* 41, 2917 (1990).
- [7] A. Gara, B. Durand, and L. Durand, *Phys. Rev. D* 40, 843 (1989).
- [8] Steve Jacobs, M. G. Olsson, and Casimir Suchyta III, *Phys. Rev. D* 33, 3338 (1986).
- [9] V. D. Mur, V. S. Popov, Yu. A. Simonov, and V. P. Yurov, *JETP* 78, 1 (1994).
- [10] M. Sadzikowski and K. Zalewski, *Z. Phys. C* 59, 677 (1993); H. Högaasen and M. Sadzikowski, Isgur-Wise functions for connected light quarks in a colour electric potential, TPJU-4/94 (hep-ph/9402279).
- [11] M. G. Olsson and Sinisa Veseli, Relativistic Flux Tube Model Calculation of the Isgur-Wise Function, UW-Madison preprint, MAD/PH/851 (hep-ph/9410249), to be published in *Phys. Rev. D*.
- [12] H. Albrecht et al., ARGUS Collaboration, *Z. Phys. C* 57, 533 (1993).

- [13] B. Barish et al., CLEO Collaboration, Measurement of the  $B \rightarrow D_1$ , Cornell Nuclear Studies Wilson Lab preprint.
- [14] C. Olson, M. G. Olsson and D. LaCourse, Phys. Rev. D **49**, 4675 (1994).
- [15] M. G. Olsson and Sinisa Veseli, The Asymmetric Flux Tube, UW-Madison preprint MAD/PH/816.
- [16] D. LaCourse and M. G. Olsson, Phys. Rev. D **39**, 2751 (1989); Collin Olson, M. G. Olsson, and Ken Williams, Phys. Rev. D **45**, 4307 (1992); M. G. Olsson and Ken Williams, Phys. Rev. D **48**, 417 (1993).
- [17] We are indebted to L. Fulcher and J. Ball for suggestions on the calculation of these matrix elements.

TABLES

Table 1: Heavy-light spin averaged states. Theoretical results are obtained from the Dirac equation with scalar confinement. Spin-averaged masses are calculated in the usual way, by taking  $\frac{3}{4}$  ( $\frac{5}{8}$ ) of the triplet and  $\frac{1}{4}$  ( $\frac{3}{8}$ ) of the singlet mass for the  $s(p)$ -waves). An estimate for the  $B_s$  was taken to be 5421 MeV, in order to make splittings  $B - B$  and  $B_s - B_s$  the same.

| state                  |                | spectroscopic label | spin-averaged | q. n.         | theory | error |   |
|------------------------|----------------|---------------------|---------------|---------------|--------|-------|---|
|                        | $J^P$          | $^{2S+1}L_J$        | mass (MeV)    | j             | k      | (MeV) |   |
| <u>cu; cd quarks</u>   |                |                     |               |               |        |       |   |
| D (1867)               | 0              | $^1S_0$             | 1S (1974)     | $\frac{1}{2}$ | 1      | 1975  | 1 |
| D (2010)               | 1              | $^3S_1$             |               |               |        |       |   |
| D <sub>1</sub> (2423)  | 1 <sup>+</sup> | $^1P_1$             | 1P (2444)     | $\frac{3}{2}$ | 2      | 2444  | 0 |
| D <sub>2</sub> (2457)  | 2 <sup>+</sup> | $^3P_2$             |               |               |        |       |   |
| <u>cs quarks</u>       |                |                     |               |               |        |       |   |
| D <sub>s</sub> (1969)  | 0              | $^1S_0$             | 1S (2075)     | $\frac{1}{2}$ | 1      | 2074  | 1 |
| D <sub>s</sub> (2110)  | 1              | $^3S_1$             |               |               |        |       |   |
| D <sub>s1</sub> (2535) | 1 <sup>+</sup> | $^1P_1$             | 1P (2559)     | $\frac{3}{2}$ | 2      | 2559  | 0 |
| D <sub>sJ</sub> (2573) | 2 <sup>+</sup> | $^3P_2$             |               |               |        |       |   |
| <u>bu; bd quarks</u>   |                |                     |               |               |        |       |   |
| B (5279)               | 0              | $^1S_0$             | 1S (5314)     | $\frac{1}{2}$ | 1      | 5313  | 1 |
| B (5325)               | 1              | $^3S_1$             |               |               |        |       |   |
| <u>bs quarks</u>       |                |                     |               |               |        |       |   |
| B <sub>s</sub> (5375)  | 0              | $^1S_0$             | 1S (5410)     | $\frac{1}{2}$ | 1      | 5411  | 1 |
| ?B <sub>s</sub> (5421) | 1              | $^3S_1$             |               |               |        |       |   |

Table 2: Heavy-light spin averaged states. Theoretical results are obtained from the no pair equation with vector confinement. Spin-averaged masses are calculated in the usual way, by taking  $\frac{3}{4}$  ( $\frac{5}{8}$ ) of the triplet and  $\frac{1}{4}$  ( $\frac{3}{8}$ ) of the singlet mass for the s(p)-waves). An estimate for the  $B_s$  was taken to be 5421 MeV, in order to make splittings  $B - B$  and  $B_s - B_s$  the same.

| state                  | spectroscopic label | spin-averaged | q. n.      | theory          | error  |
|------------------------|---------------------|---------------|------------|-----------------|--------|
|                        | $J^P$               | $^{2S+1}L_J$  | mass (MeV) | j k             | (MeV)  |
| <u>cu; cd quarks</u>   |                     |               |            |                 |        |
| D (1867)               | 0                   | $^1S_0$       | 1S (1974)  | $\frac{1}{2}$ 1 | 1978 4 |
| D (2010)               | 1                   | $^3S_1$       |            |                 |        |
| D <sub>1</sub> (2423)  | 1 <sup>+</sup>      | $^1P_1$       | 1P (2444)  | $\frac{3}{2}$ 2 | 2440 4 |
| D <sub>2</sub> (2457)  | 2 <sup>+</sup>      | $^3P_2$       |            |                 |        |
| <u>cs quarks</u>       |                     |               |            |                 |        |
| D <sub>s</sub> (1969)  | 0                   | $^1S_0$       | 1S (2075)  | $\frac{1}{2}$ 1 | 2072 3 |
| D <sub>s</sub> (2110)  | 1                   | $^3S_1$       |            |                 |        |
| D <sub>s1</sub> (2535) | 1 <sup>+</sup>      | $^1P_1$       | 1P (2559)  | $\frac{3}{2}$ 2 | 2562 3 |
| D <sub>sJ</sub> (2573) | 2 <sup>+</sup>      | $^3P_2$       |            |                 |        |
| <u>bu; bd quarks</u>   |                     |               |            |                 |        |
| B (5279)               | 0                   | $^1S_0$       | 1S (5314)  | $\frac{1}{2}$ 1 | 5315 1 |
| B (5325)               | 1                   | $^3S_1$       |            |                 |        |
| <u>bs quarks</u>       |                     |               |            |                 |        |
| B <sub>s</sub> (5375)  | 0                   | $^1S_0$       | 1S (5410)  | $\frac{1}{2}$ 1 | 5409 1 |
| ?B <sub>s</sub> (5421) | 1                   | $^3S_1$       |            |                 |        |

## FIGURES

Figure 1: S-wave classical turning points for the Dirac equation with scalar confinement.

Figure 2: S-wave classical turning points for the Dirac equation with vector confinement.

Figure 3: S-wave classical turning points for the no pair equation. Note that there is no difference between the scalar and the vector confinement.

Figure 4: Dependence on  $\mu$  of the three lowest positive energy states for the pure Coulomb case with  $m = 1 \text{ GeV}$ ;  $\alpha = 0.5$ ;  $k = 1$  and  $j = \frac{1}{2}$ . Exact solutions of the Dirac equation are shown by full lines, while our variational solutions are shown by dashed lines (shorter for  $N = 15$  and longer for  $N = 25$  basis states used).

Figure 5: Scaled eigenvalue  $\lambda$  for the ground state ( $j = \frac{1}{2}$ ;  $k = 1$ ). We used  $m = 1 \text{ GeV}$  and  $N = 25$  basis states. The no pair equation result is shown by the dashed line, while the Dirac equation result is shown by the full line.

Figure 6: Dependence on  $\mu$  of the three lowest positive energy states and the three highest negative energy states for the Dirac equation with scalar confinement, with  $m_q = 0.3 \text{ GeV}$ ;  $a = 0.2 \text{ GeV}^2$ ;  $\alpha = 0.5$ ;  $k = 1$  and  $j = \frac{1}{2}$ . Full lines correspond to  $N = 25$ , and dashed lines correspond to  $N = 15$  basis states used.

Figure 7: Regge trajectories for the Dirac equation with scalar confinement. We have chosen  $m_{u,d} = 0$ ;  $a = 0.2 \text{ GeV}^2$ , and  $\alpha = 0.5$ . Full lines correspond to  $k = j + \frac{1}{2}$ , and dashed lines to  $k = j + \frac{1}{2}$ . To ensure that all calculated energies are correct, we used  $N = 100$  basis states, and kept first 15 states.



Figure 8:  $\mathbb{W}$  function for B decays calculated from the Dirac equation with scalar confinement. Values for the light quark mass  $m_{u,d}$ , tension  $a$  and short range potential constant  $\kappa$  are taken from the (50). For the sake of clarity, error bars are shown only for the CLEO data.

Figure 9: Dependence on  $\beta$  of the three lowest positive energy states and the three highest negative energy states for the Dirac equation with vector confinement, with  $m_q = 0.3 \text{ GeV}$ ;  $a = 0.2 \text{ GeV}^2$ ;  $\kappa = 0.5$ ;  $k = 1$  and  $j = \frac{1}{2}$ . We used  $N = 15$  basis states. The mixing between positive and negative states is evident.

Figure 10: Dependence on  $\beta$  of the three lowest positive energy states and the three highest negative energy states for the no pair equation with vector confinement, with  $m_q = 0.3 \text{ GeV}$ ;  $a = 0.2 \text{ GeV}^2$ ;  $\kappa = 0.5$ ;  $k = 1$  and  $j = \frac{1}{2}$ . Full lines correspond to  $N = 25$ , and dashed lines correspond to  $N = 15$  basis states used.

Figure 11: Regge trajectories for the no pair equation with vector confinement. We have chosen  $m_{u,d} = 0.3 \text{ GeV}$ ;  $a = 0.2 \text{ GeV}^2$ , and  $\kappa = 0.5$ . Full lines correspond to  $k = (j + \frac{1}{2})$ , and dashed lines to  $k = j + \frac{1}{2}$ . To ensure that all calculated energies are correct, we used  $N = 50$  basis states, and kept first 10 states.

Figure 12:  $\mathbb{W}$  function for B decays calculated from the no pair equation with vector confinement. Values for the light quark mass  $m_{u,d}$ , tension  $a$  and short range potential constant  $\kappa$  are taken from (57). For the sake of clarity, error bars are shown only for the CLEO data.

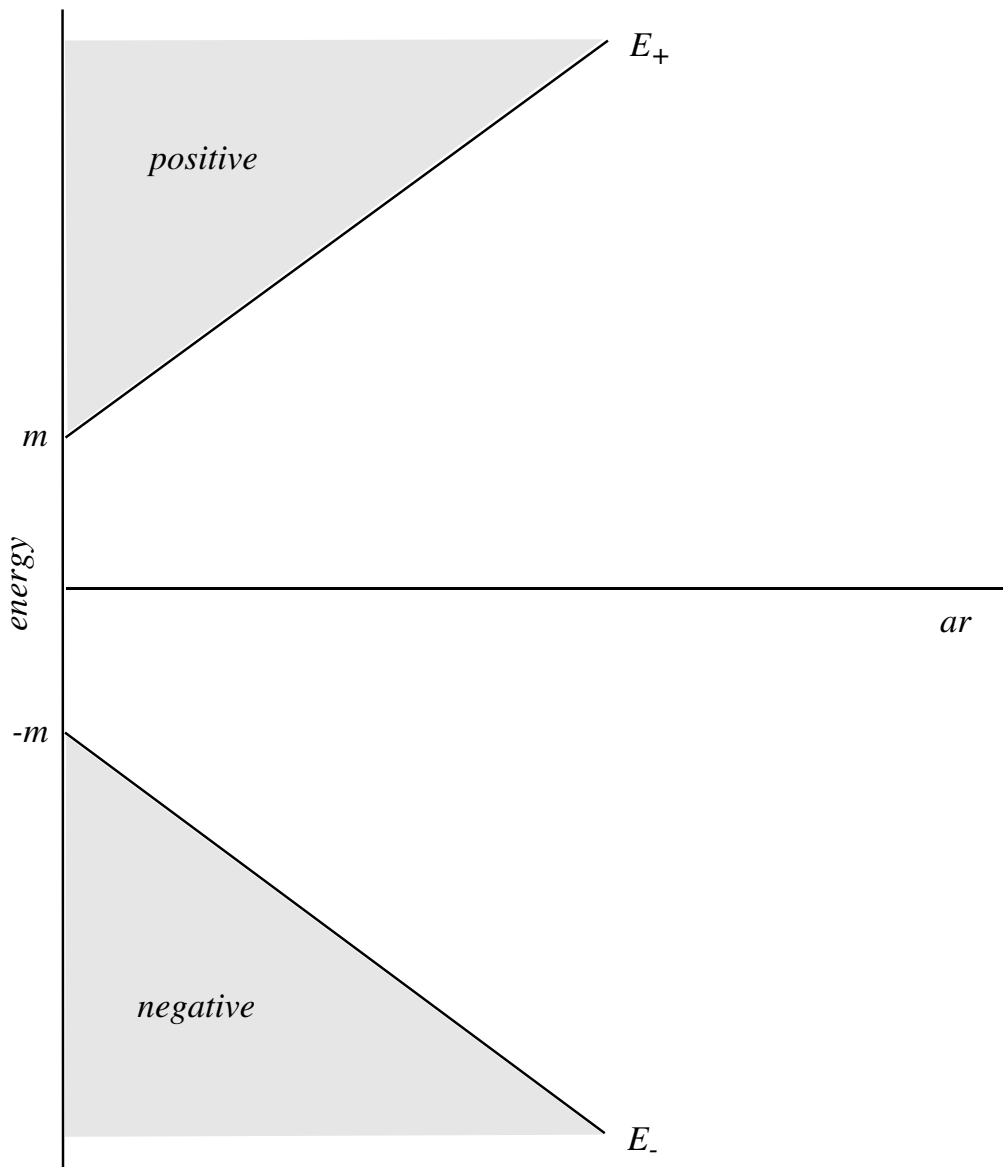


Figure 1

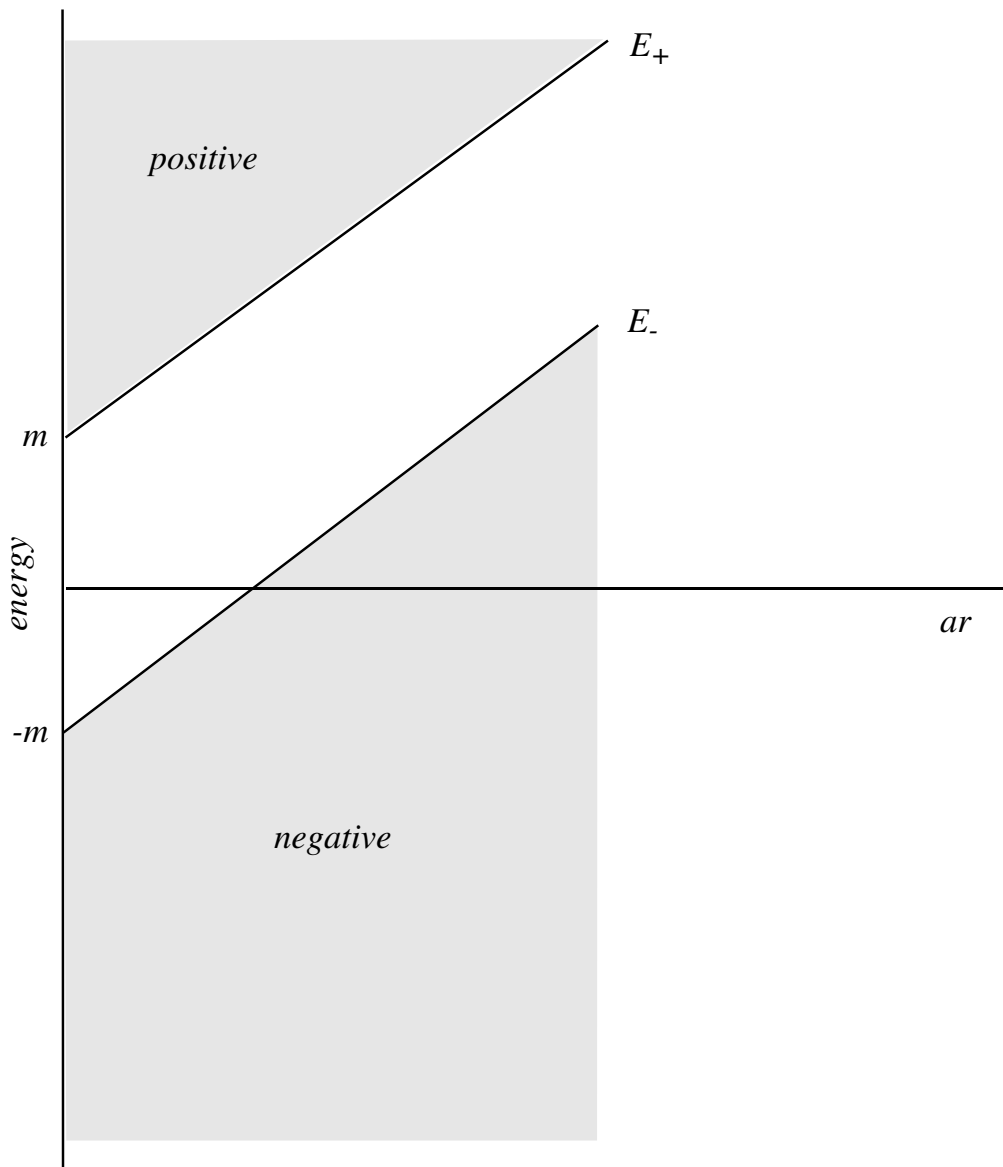


Figure 2

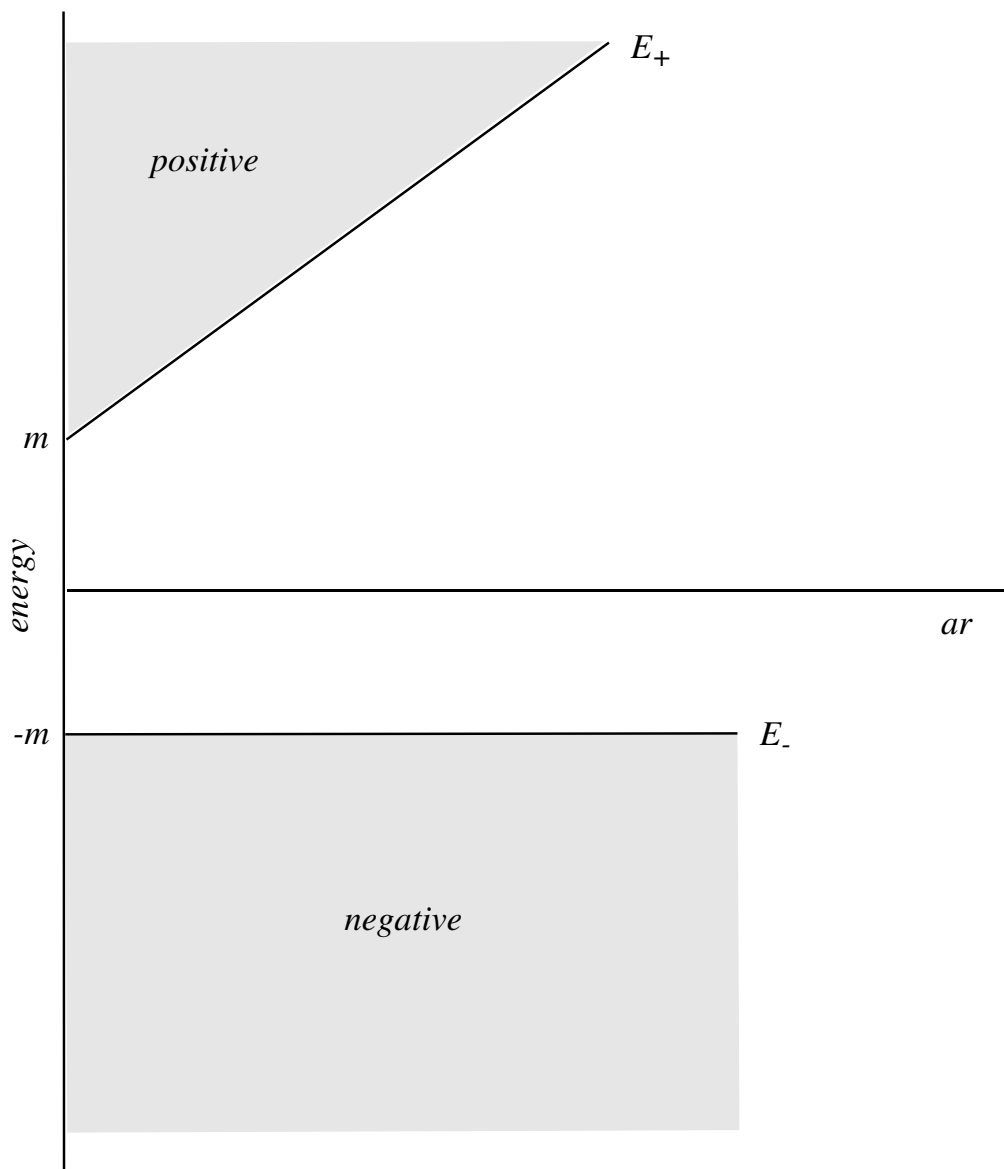


Figure 3

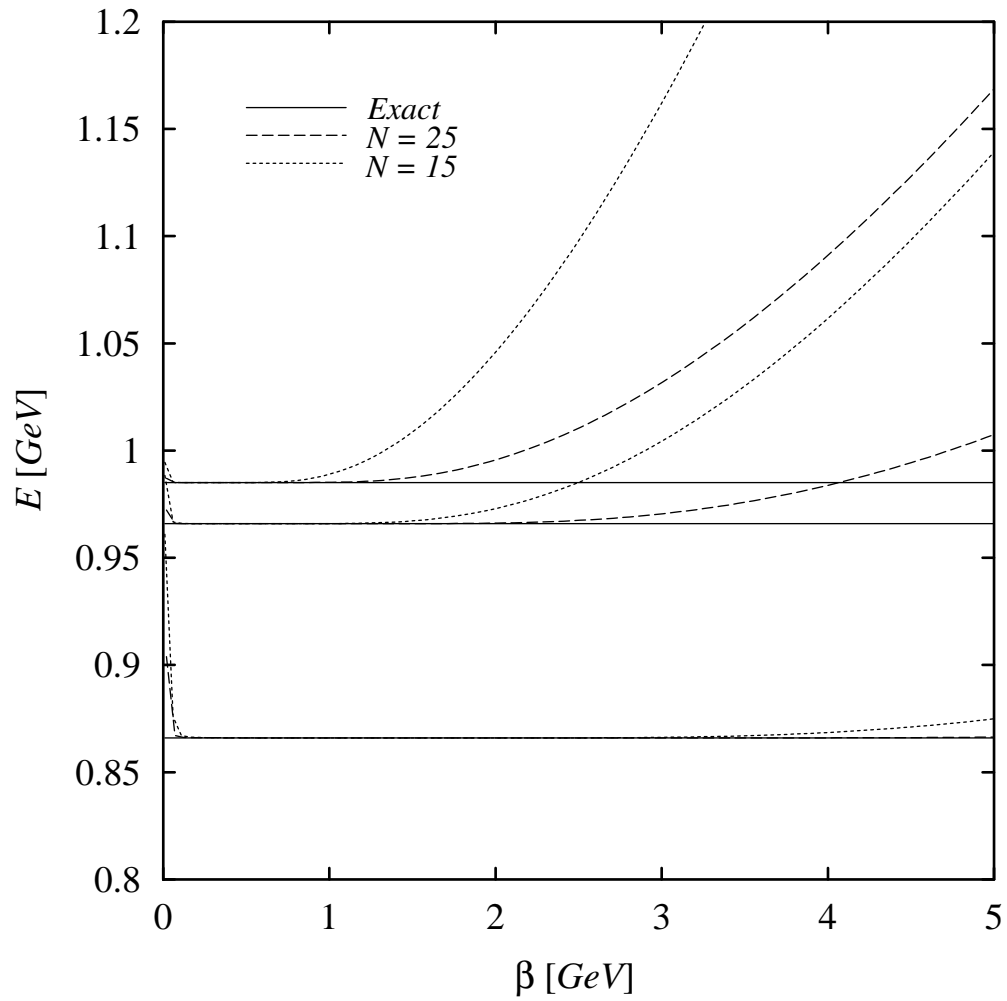


Figure 4

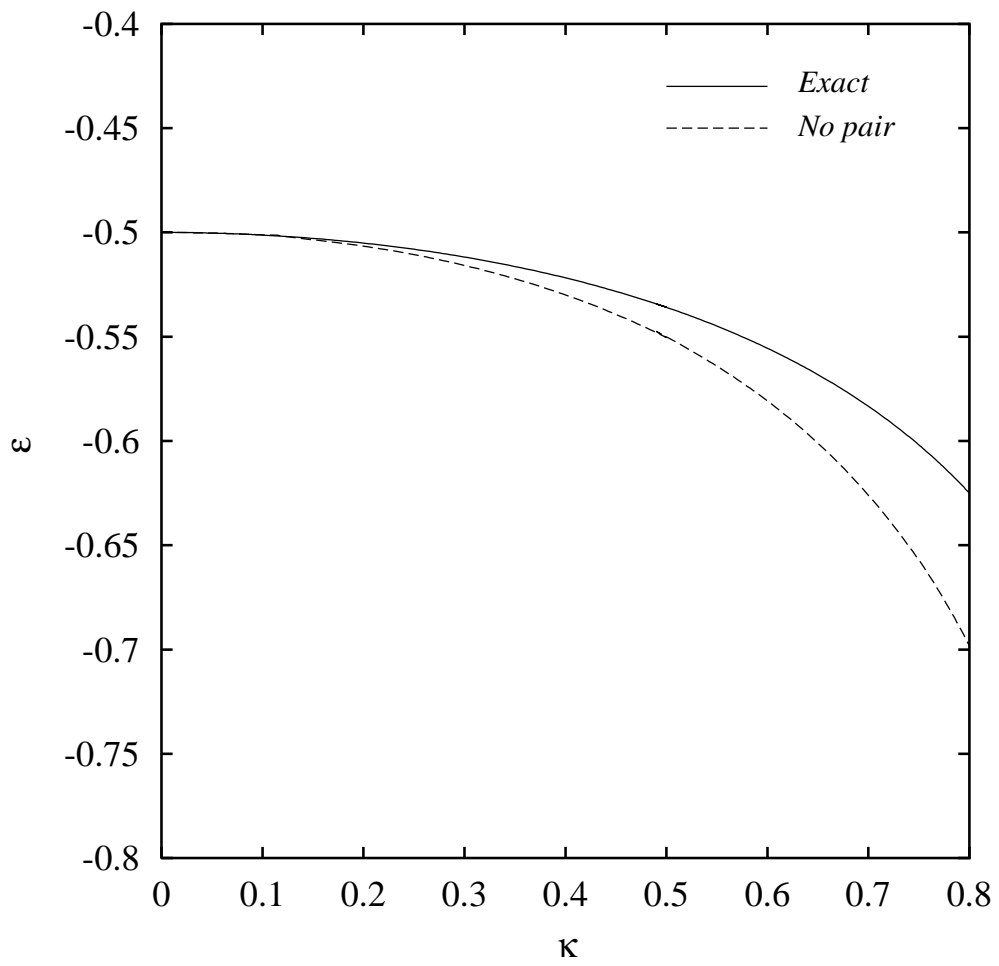


Figure 5

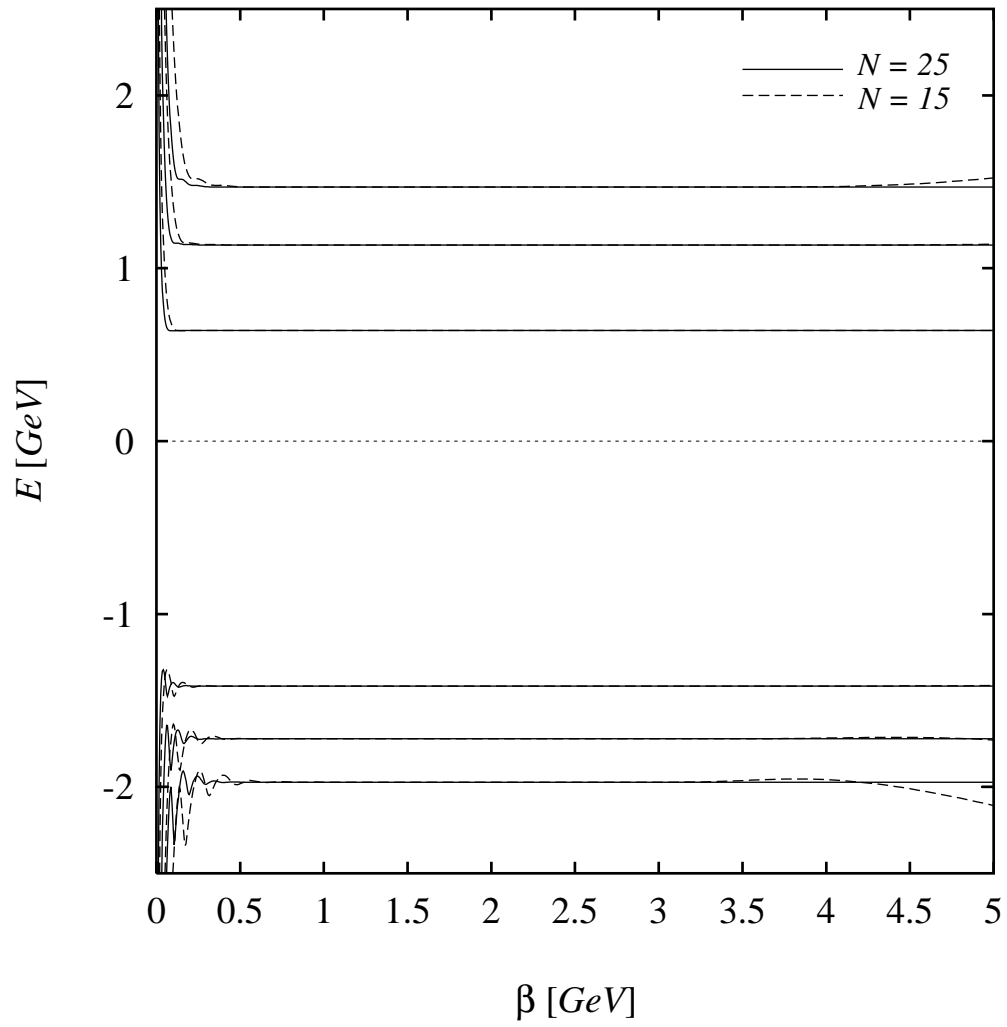


Figure 6

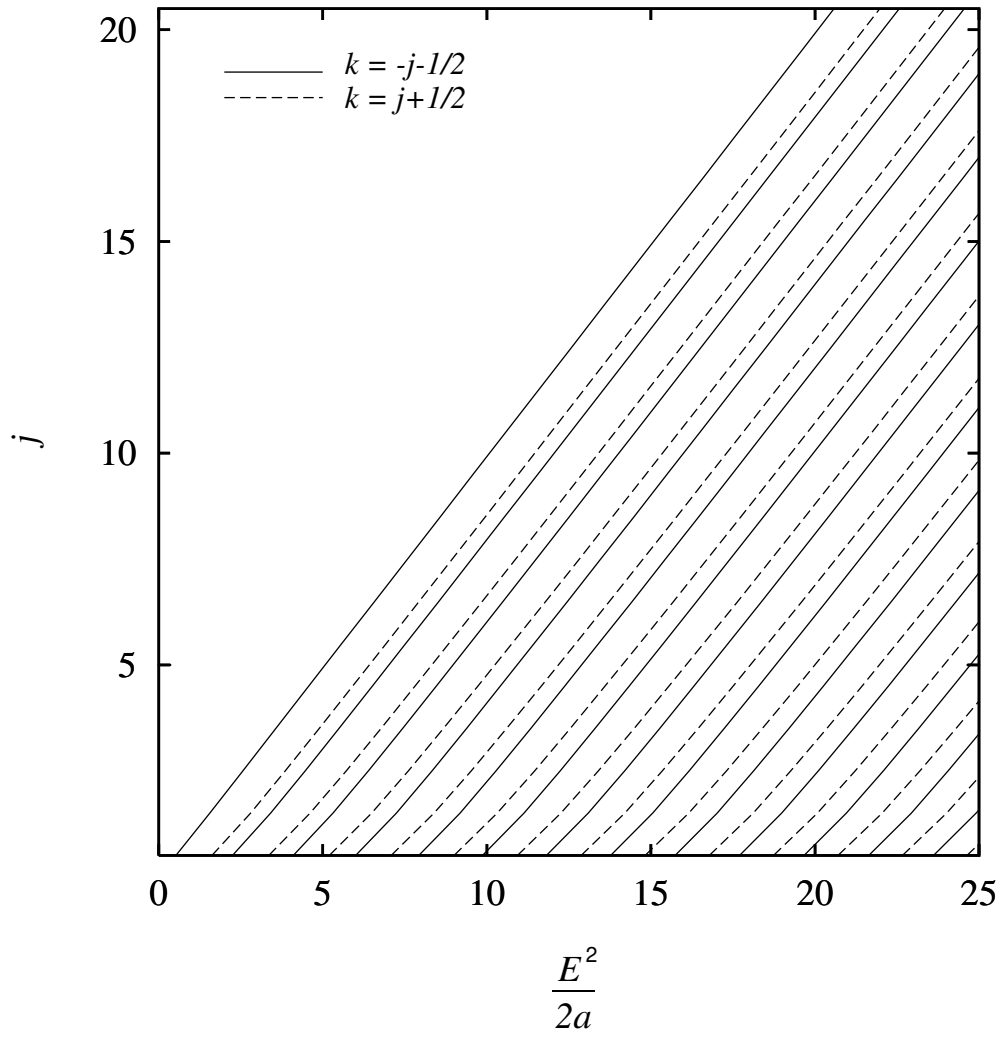


Figure 7



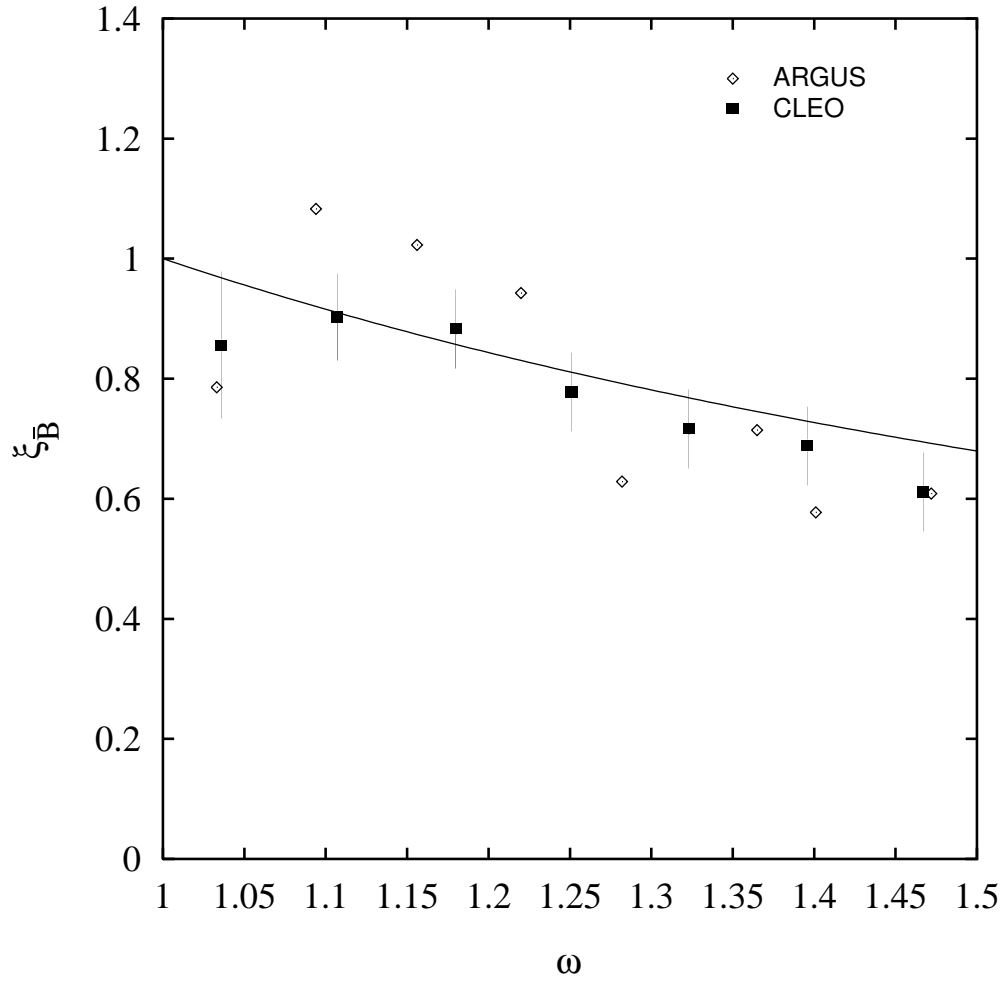


Figure 8

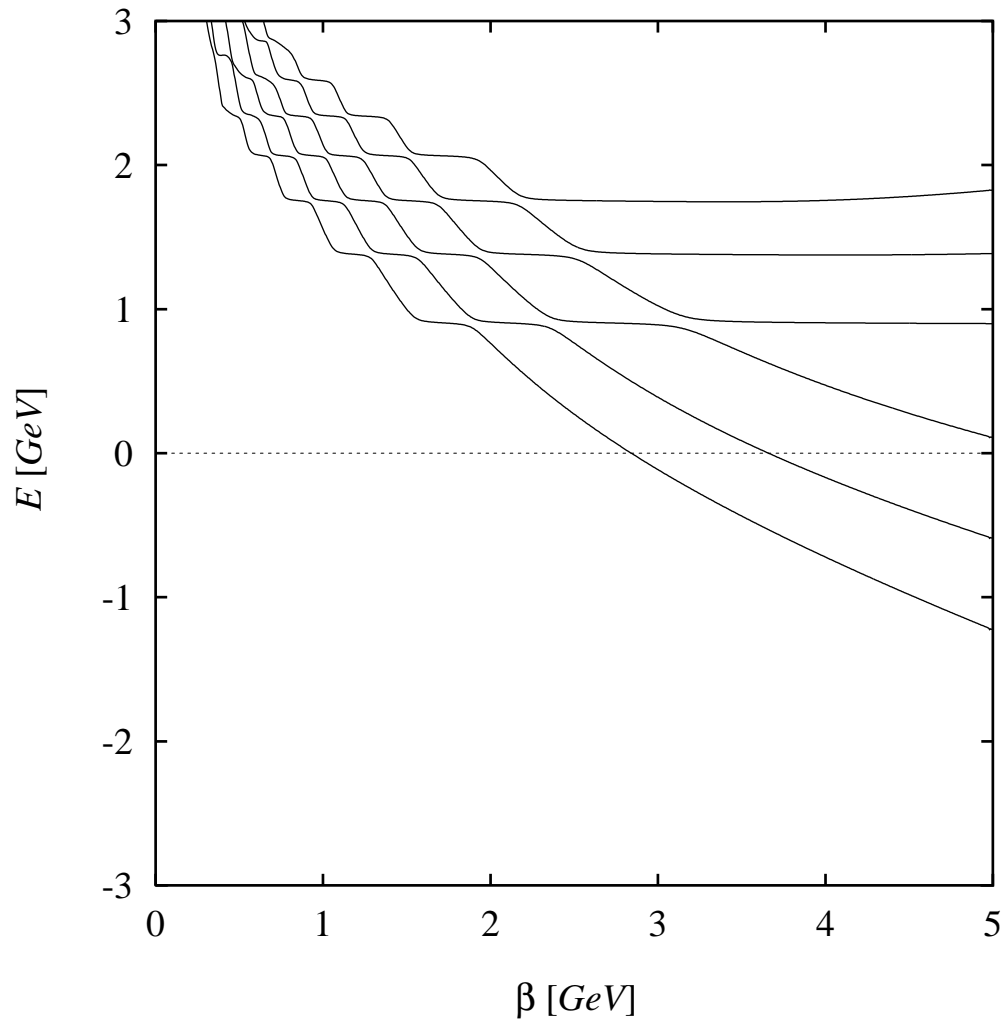


Figure 9

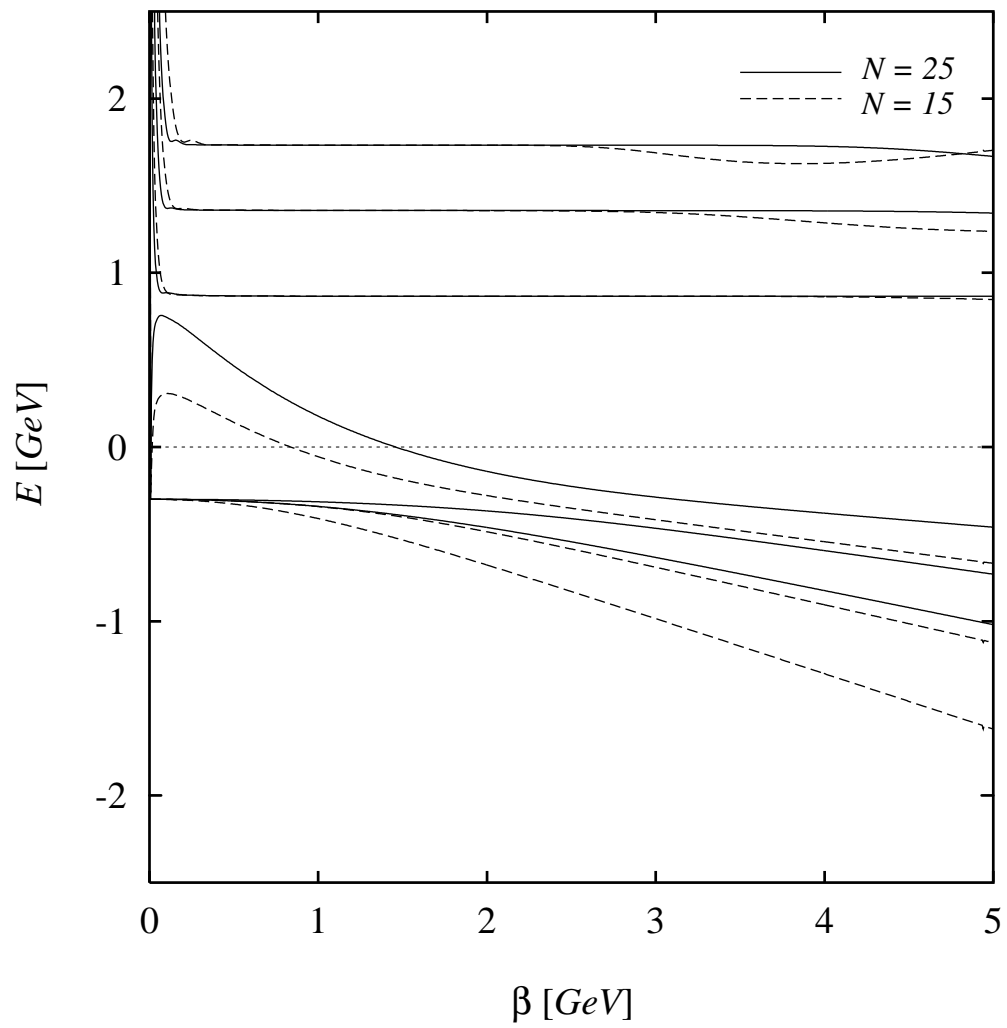


Figure 10

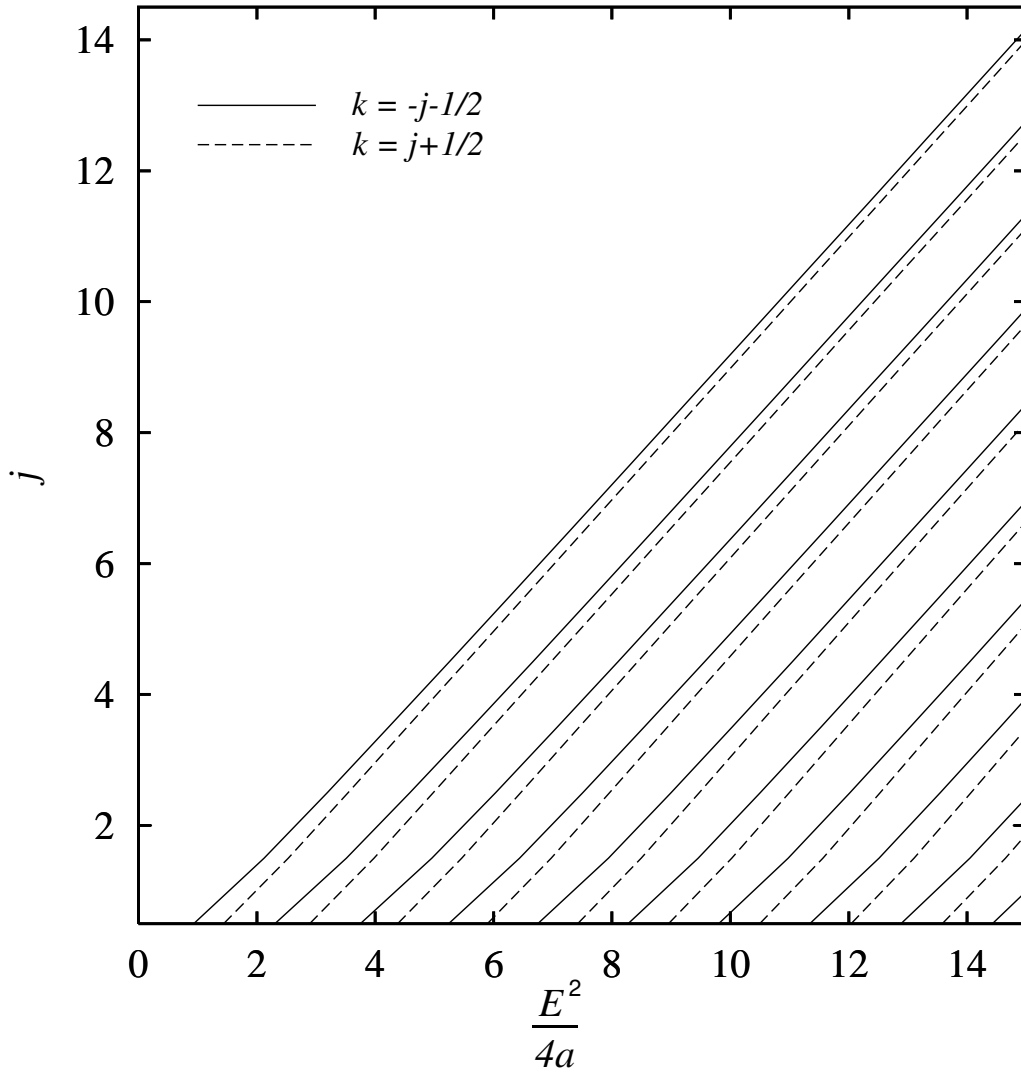


Figure 11

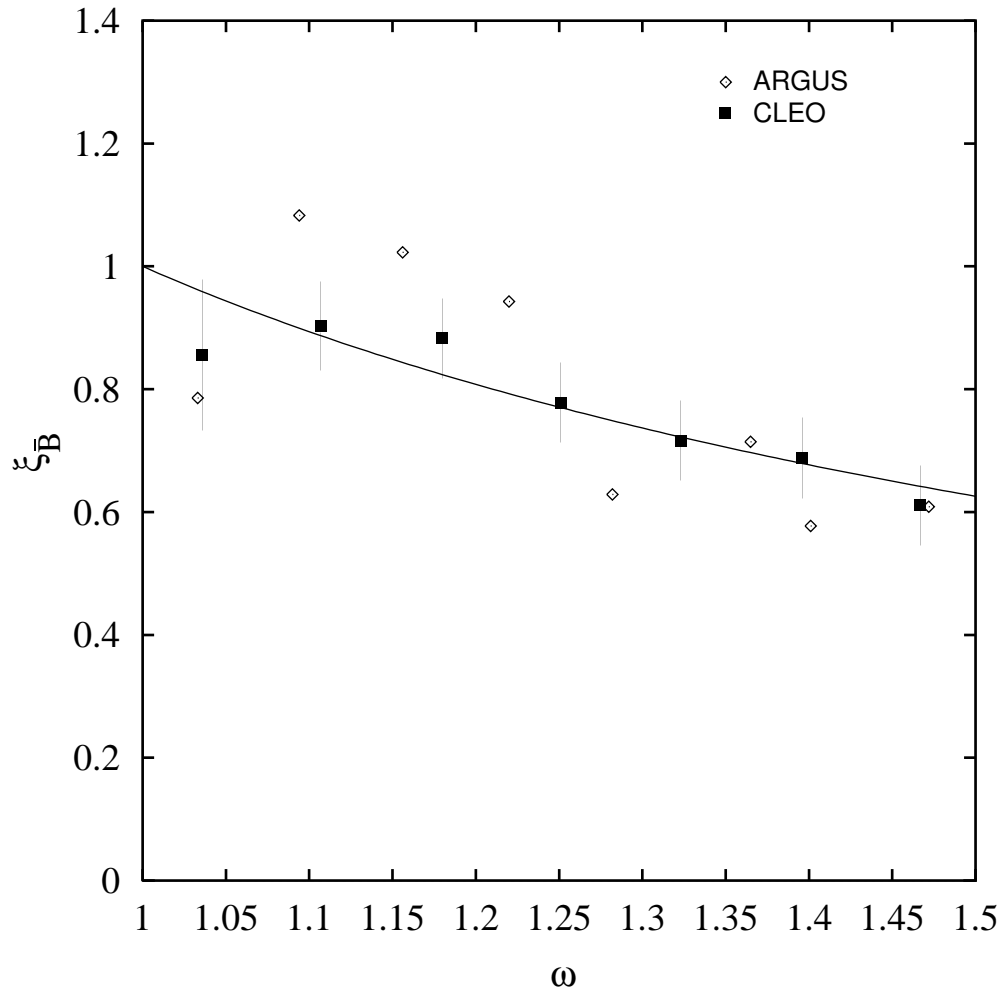


Figure 12